This is a peer-reviewed, accepted author manuscript of the following research article: Kodakkadan, YNV, Maslen, C, Cigler, P, Štěpánek, F & Rehor, I 2021, 'Friction-directed self-assembly of Janus lithographic microgels into anisotropic 2D structures', Journal of Materials Chemistry B, vol. 9, no. 23, pp. 4718-4725. https://doi.org/10.1039/D1TB00572C

Friction-Directed Self-Assembly of Janus Lithographic Microgels into Anisotropic 2D Structures

Yadu Nath Vakkipurath Kodakkadan, [a] Charlie Maslen, [a] Petr Cigler, [b] Frantisek Stepanek, [a] Ivan Rehor*[,a,b]

We present a method for creating ordered 2D structures with material anisotropy from self-assembling micro-sized hydrogel particles (microgels). Microgel platelets of polygonal shapes (hexagon, square, rhombus), obtained by a continuous scalable lithographic process are suspended in an aqueous environment and sediment on an inclined plane. As a consequence of gravitational pull, they slide over the plane. Each half of the microgel is composed of a different type of hydrogel [poly(*N*-isopropylacrylamide) – PNIPAM, and poly(ethylene glycol) diacrylate, respectively] which exhibit different frictional coefficients when sheared over a substrate. Hence microgels self-orientate as they slide, the side with the lower frictional coefficient positions in the direction of sliding. The self-oriented microgels concentrate at the bottom of the tilted plane. Here they form densely packed structures with translational as well as orientation order

Introduction

Pick-and-place methods are prevalent in industrial processes for organizing smaller objects to larger structures but are challenged in microscale by multiple factors such as limited positioning precision, adhesion forces, or achievable throughput[1–4]. In contrast, molecular[5] and nanosized[6] systems are organized through bottom-up self-assembly (SA) processes. Transferring a SA process to microscale (10-1000 µm) represents a great opportunity for microfabrication since the parallel nature of SA would provide scalable, low-cost production of photonic materials, mechanical metamaterials or assembly of electronics[,2,4,7–12].

During molecular/nanoparticle SA processes, the constituent building blocks constantly move and rearrange due to Brownian motion and ultimately converge towards an (ordered) state corresponding to a (local) free energy minimum[6]. The equilibrium state is controlled by interactions between the building blocks, that are encoded in their shape[13] or material makeup[14,15] as well as their environment (confinement, templating, external fields)[16]. However, when the building block size is greater than several microns (so-called mesoscale self-assembly - MESA[1,17]), the thermal fluctuations average out over the size of the block, and the Brownian motion vanishes. Such system cannot spontaneously overcome local energy minima and explore its phase space. Thermal fluctuations as the source of motion can be replaced by mechanical agitation (stirring, ultrasound) to enable self-assembly of micro and macroscopic building blocks[1,4,10,18–22]. This has been demonstrated with relatively simple systems, such as spherical building blocks, which form periodic dense packings when agitated under confinement[19,23]. In 2D, experimental and theoretical work has also been conducted focusing on arrangements and interactions of polar particles on vibrating plate, whose behaviour relates to that of active matter[24,25].

The introduction of attractive capillary[26] and depletion forces[27] can be used to align the building blocks, once in contact, to maximize their contact area. These interactions have been used to self-assemble prismatic building blocks into densely packed arrangements[7,28] or to form pairs from complementary lock-and-key building blocks[22].

In cases where the SA process is, to a certain extent, realized by the environment, the process is often denoted directed assembly[16]. The use of external fields (magnetic[29], electric[30], or acoustic[31]) for building block (pre)organization is one example. Alternatively, the building blocks interact with physical features in their surroundings that navigate their paths[32] or are responsible for their ultimate arrangement[33]. Additionally, the deployment of the building blocks close to the desired final positions has been utilized to provide complex ordered structures[34]. Furthermore, the building blocks can be actively navigated and steered in the environment, either by viscous forces ('fluidic assembly'[35,36]), electric field ('dielectrophoretic

[a] University of Chemistry and Technology Prague, Faculty of Chemical Engineering,Technicka 5, 166 28 Prague 6, Czech Republic.
[b] Institute of Organic Chemistry and Biochemistry of the Czech Academy of Sciences, Flemingovo nam. 2, 160 00, Prague, Czech Republic
* e-mail: ivan.rehor@vscht.cz

† Footnotes relating to the title and/or authors should appear here.
Electronic Supplementary Information (ESI) available: [details of any supplementary information available should be included here]. See DOI: 10.1039/x0xx00000x

assembly'[37]), or light ('optical induced dielectrophoresis'[38]). These last-listed methods, however, are more representative of a top-down approach ('tool directed') than bottom-up ('process directed')[2] and as such typically lack parallel nature and concomitant scalability of the SA. In summary, it appears that there is a direct pay-off between the achievable complexity of the resulting assembly and the need for involvement of the external environment, acting during the SA process.

Here we present a novel microfabrication method for periodic, materially anisotropic hydrogel sheets, based on SA of Janus-like building blocks under gravity-induced confinement. The microgels dimensions are far above the Brownian limit, however, structures with translational and rotational order can spontaneously form without agitation, or any additional force to gravity (which is inherently present in the system). The translational order is a result of a global potential energy well. Self-orientation is responsible for the rotational order in the structures and is achieved by non-uniform friction distribution over the building block – bottom contact plane.

We provide a proof of concept data, showing that assembled microgels can be covalently bound together into a single sheetthat provide anisotropic volumetric response when subjected to heating.

Experimental Section

Materials

Ethylene glycol diacrylate (EGDA; M_n ~700), *N*-isopropylacrylamide (NIPAM) and acryloxyethyl thiocarbamoyl Rhodamine B (Rh-Ac) was purchased from Sigma Aldrich. The photoinitiator lithium phenyl-2,4,6-trimethylbenzoylphosphinate (LAP) was synthesized according to previously published procedure[39]. A SYLGARD 184 elastomer kit was used to produce the polydimethylsiloxane (PDMS) channel and the cuvette surface coating. PS cuvettes were purchased from Dow Corning.

Pregel solution composition

Pregel solution 1: 30 mg of EGDA was dissolved in 70 µl of Millipore water. 2 mg (6.8 µmol) of LAP photoinitiator was added. *Pregel solution 2*: 37 mg of NIPAM was dissolved in 100 µl of Millipore water, then 20 mg of EGDA together with 2 mg of LAP was added.

Rh-Ac was added (4 µL of a DMSO stock solution of concentration 4 mg/mL) to one of the solutions. Each solution was sonicated to dissolve the LAP and centrifuged to remove insoluble contaminants (10 min at 10,000 *g*).

Stop-Flow Lithography

The multiple stream stop-flow lithographic microgel preparation has been previously described[40,41]. The two solutions were injected through two separate inlets of the microfluidic chip. A flow was induced by generating a pressure difference using compressed air. UV light was used to crosslink the solution so that the boundary between the two parallel flows lies at the center of the formed hydrogel microparticles (microgels). A photomask (hexagon, square, rhombus, disc, elongated hexagon) was used to make microgels of desired shapes.

The microgels were flushed and collected in a PCR tube, and then washed to remove the non-crosslinked pregel solution. A mixture of surfactant (1% Pluronic F127 and 1% Tween 20) solution was used to keep the microgels from aggregating.

Self-Assembly Experiments

The SA experiments were done in a polystyrene cuvette, in which the internal surface is spin-coated with a PDMS solution and subsequently cured. The cuvette was filled with aqueous surfactant solution (1% w/w Tween 20 and 1% w/w Pluronic F-127) and the microgels were suspended at the side wall. The cuvette was then set to a defined angle of inclination (3°, 6°, 9°, 12°). The experiments were carried over 48 hours.

Cuvette coating

Before use the cuvettes were washed thoroughly with deionized water and all the experiments were conducted inside a dust-free laminar flow box. The PDMS solution was made by mixing the silicon elastomer base and the curing agent at a ratio of 1:7. The solution was mixed and centrifuged to remove air bubbles. The PDMS solution was coated using a spin coater at speed of 1500 rpm for 2 min. The PDMS coating was cured at 70 °C overnight with the cuvette kept bottom-up during curing.

Microgel Binding

Permanent binding of the microgel assemblies was done using exposure to UV light and photo-crosslinking. First, the solution containing the assembled microgels was exchanged with a 2% w/w LAP photo initiator solution in water. The cuvette was covered to prevent any exposure to light and stored overnight for uniform diffusion throughout the solution. UV light was exposed through a mask at an intensity of 45 mW/cm^2 which initiated crosslinking between the microgels, forming a single sheet. The hydrogel sheet was then washed with water 4 times to completely remove the residual LAP. The sheet was heated to 70° C and then cooled back to RT under simultaneous microscopic observation. Since the heating apparatus blocked the diascopic illumination of the heated sample, the observation was conducted in episcopic fluorescence mode.

Result and Discussion

Friction Induced Self-Orientation

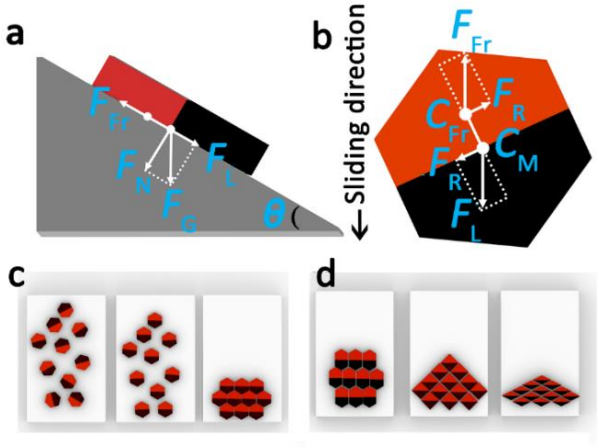

Fig. 1. (a) Schematic diagram showing the forces acting on a Janus microgel sliding over a tilted plane. (b) Forces acting on the sliding microgel, responsible for its self-orientation. (c) Schematics of the self-orientation and self-assembly process, for hexagons. (d) Self-assembly of other microgel shapes.

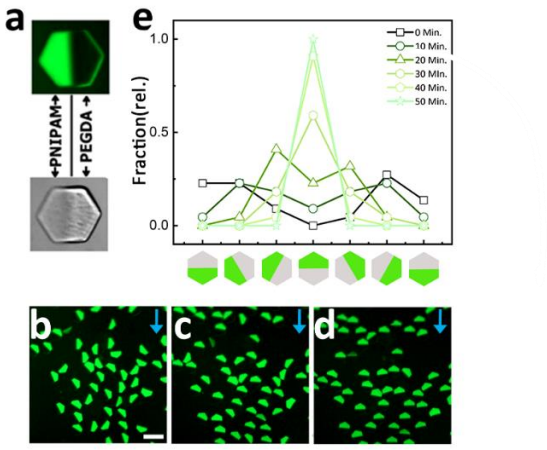

Fig. 2. Self-orientation of sliding Janus hexagons. (a) Individual particle: in which PNIPAM side is fluorescently labeled. Images of gradually self-orienting hexagons with a random initial orientation at (b) 0 min, (c) 30 min, (d) 50 min (the blue arrow indicates direction of sedimentation, scale bar corresponds to 200 µm). (e) The relative distributions of the hexagon orientations with respect to the slope, ordered from the darkest to the lightest color (square 0 min, circle 10 min, triangle 20 min, hexagon 30 min, pentagon 40 min, and star 50 min).

In this study we control the orientation of lithographic microgels, sliding over a tilted plane via anisotropic friction distribution along the sheared plane of the Janus microgel. The microgels are of uniform thickness and can be fabricated in arbitrary shapes in lateral dimensions, by scalable continuous process stop-flow lithography[41–43].

A microgel on a tilted plane is subjected to the component of the gravitational force running parallel to the surface (lateral force F_L) which is responsible for its sliding motion. This force is counteracted by a friction force (F_{Fr}) and these two are in equilibrium (Fig. 1a). We neglect the viscous drag force acting on the sliding microgel, as it is significantly smaller than the friction force (justification is presented in the ref. [44]). The friction force in sheared polymeric material depends on the shear velocity. The swollen polymer chains adapt to the shear stress by conformational changes and the friction force grows with the shear velocity in an analogy to the viscous drag force[45–47] (the polymer chains flow over the surface, being separated by a thin lubricating solvent layer). The scaling is typically linear (analogy to Newtonian fluids) at low sheer speeds changing to sub-linear at high sheer speeds (analogy to shear-thinning fluids)[45]. For Newtonian behavior, the sliding velocity of a microgel can be obtained by equating the frictional force to the gravity force component parallel to the substrate. This gives the following expression for the sliding velocity v as a function of the friction coefficient f, tilt angle ϑ, and the buoyant mass m of the microgel with sheared area S[44]:

$$v = \frac{m\, g\, \sin\theta}{S\, f} \qquad (1)$$

We tested the behaviour of single-phase microgels (hexagons, distance between the opposite vertexes = 115 µm) composed from single-phase poly(*N*-isopropylacrylamide) (PNIPAM) and poly(ethylene glycol) diacrylate (PEGDA) when subjected to shear by allowing them to slide along surfaces tilted at various angles (Fig. S1). As expected, the microgels slide at a constant velocity at a fixed angle with the sliding velocity scaling approximately linearly with the lateral force, for the angles 3°, 6°, and 9° according to the Eq. (1). In the case of pure PEGDA microgels, we observed a steep increase of the sliding velocity when the tilt angle is increased from 9° to 12°. This increase is likely caused by the transition from the Newtonian to the shear-thinning behaviour, often observed with increasing shear velocity[45].

With a microgel of uniform composition, each section of its sheared surface exhibits uniform friction properties and, hence, the local friction pressure at any point of contact is identical to the average friction pressure (F_{Fr}/S). Estimating a mean location of the distribution of friction over the sheared plane provides a point, we call 'center of friction (C_{Fr})' in an analogy to the center of mass (C_M). The resulting friction force exerted on the sliding microgel is allocated to this point. For a uniform composition microgel, this center of friction lies in the geometric center of its bottom (sheared) plane which is identical to the projection of the center of mass to this plane. Since the lateral component of the gravity force and the friction force act at the same point in a uniform microgel, such microgel slides at any lateral orientation with respect to the sliding direction and will not rotate. However, if the distribution of local friction pressure is non-uniform (such as if the microgel is composed of several segments of different composition), the center of friction and the center of mass have different locations on the sheared plane. As a result, a torque drives the reorientation of the

particle, such that the line center of mass - center of friction aligns with the direction of the slope (Fig. 1 b, c).

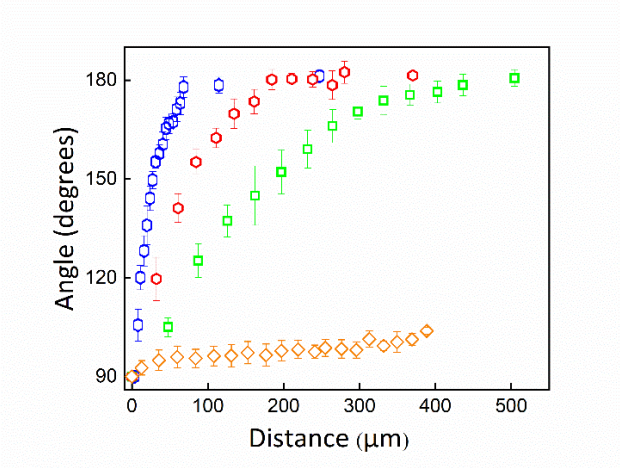

Fig. 3. Reorientation rates of various shapes, sliding at 6° tilt. Elongated hexagon (blue elongated hexagon), hexagon (red hexagon), square (green square), rhombus (orange rhombus). The error bars represent standard deviation from 10 experiments.

Indeed, in the experiments, the Janus hexagons (opposite vertex distance 115 μm) composed of two halves with different friction coefficient (PEGDA and PNIPAM hydrogel respectively) self-oriented when subjected to sliding (Fig. 2) until their lower friction PEGDA side positioned in the direction of the slope (Fig. 2, Fig. S2, video S1). The microgels self-oriented, in this manner at tilt angles up to 10° (discussed in Supplementary text S1, Fig. S3). The sliding speeds of the Janus hexagons were 0.05, 0.23 and 0.44 μm/s at 3°, 6° and 9° incline respectively (Fig S1).

The particle geometry affects the self-orientation rates (Fig. 3). Elongation of the particle in the direction of the center of mass – center of friction axis results in a greater separation of these two points and, thus, increases the torque and accelerates the reorientation (for a full justification see Supplementary text S2). The center of mass-center of friction separation in square-shaped Janus microgels is somewhat shorter than in hexagons, which caused their slower reorientation, compared to the hexagons. The separation in rhombic shape is even shorter, which resulted in no self-orientation of rhombuses, observed over the timescale of the experiment. All the separations are derived in Supplementary text S2.

Self-Assembly of Janus Building Blocks

The ability of microgels to self-orientate is utilized to control their orientation during their self-assembly into periodic structures. All the microgel shapes in this study were designed to orientate so that one vertex points in the sliding direction. This orientation facilitates their assembly to the densest packings at the bottom – the vertex allows a microgel to squeeze between others, pushing them aside (video S2). In experiments, the hexagons form densely packed hexagonal crystalline sheets with, predominantly, preserved orientation of the Janus boundary (Fig. 4, video S3).

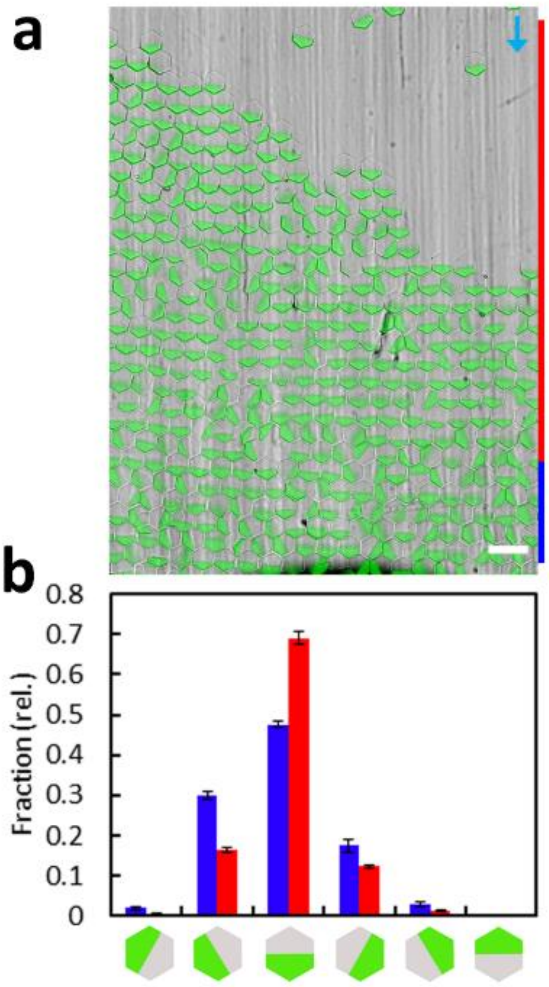

Fig. 4. (a) Densely packed Janus hexagons with predominantly aligned Janus boundaries – PEGDA side is fluorescently labelled (the blue arrow indicates the direction of sedimentation, blue line indicates bottom five rows, red line indicates rest of the assembly, scale bar corresponds to 200 μm). (b) Hexagon orientation distributions in the bottommost five rows (blue) and the rest of the assembly (red) respectively.

Below, we qualitatively describe the dynamics of the SA process, that occurs in two phases – untemplated and templated growth. The first hexagon particles that reach the bottom of the well get randomly oriented there – some tip over to the edge to align one hexagon edge with the flat well bottom, and some remain standing at the vertex being supported by adjacent hexagons. As a consequence, the first several rows of sedimented hexagons are randomly assembled, without translational order (Fig. 4a). This random assembly is rather fluidic since the hexagons have mainly point contacts with their neighbours (Fig. 5a). As new hexagons reach the assembly, they apply gravitational load on the hexagons below which causes displacements in the fluidic structure (Fig. 5b, c, d). Occasionally, a densely packed crystalline domain is formed as a result of these displacements (Fig. 5e). The rigidity of this domain is significantly higher than that of the surrounding

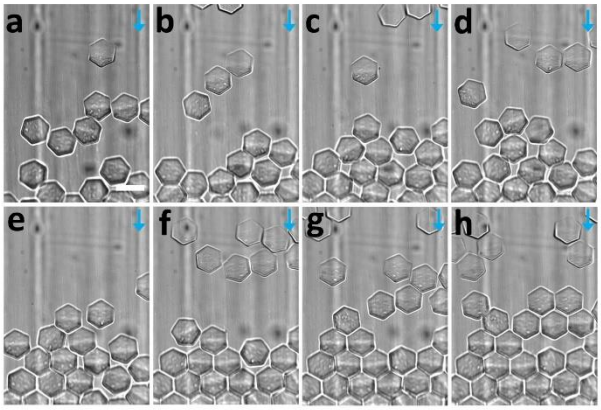

Fig. 5. Crystallization of the fluidic assembly. The blue arrows indicate direction of sedimentation and the scale bar corresponds to 100µm.

random assembly and is rarely broken once formed. Through this process, the whole assembly gradually turns crystalline (Fig. 5f) with only a few defects at the boundaries between individual domains. Once the bottom of the well crystallizes, it serves as a template to which the newly sliding self-oriented hexagons are instantaneously incorporated (Fig. 5g,h). This proposed two-step mechanism also explains the higher abundance of hexagons with a misoriented Janus boundary in several bottom-most layers, compared to the rest of the assembly (Fig. 4a). The initial rearrangements in the random fluidic assembly are responsible for the greater degree of randomization of the microgel orientation, while during the templated growth process, this orientation is preserved to a significantly greater degree.

Even the section of the structure, that resulted from the templated growth, contains about 30 % of hexagons with misoriented Janus boundaries (Fig. 4a), despite almost perfect hexagon self-orientation (>95 % of hexagons oriented within ± 30°) during the sliding. The hexagon misorientation occurs during their mutual interactions in the assembly. Below we qualitatively discuss the main misorientation mechanisms. Firstly, some microgel misoriented during the incorporation into the structure by tipping over (Fig. 6, video S4). The second mechanism is the redistribution of microgels along the well width. This redistribution is a result of the non-uniform population distribution of the sliding microgels along the width

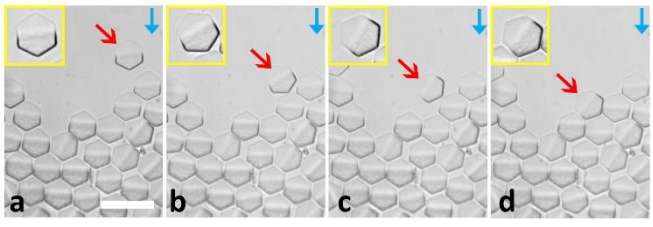

Fig. 6. Orientation loss during the incorporation into the structure. The blue arrows indicate direction of sedimentation and the scale bar corresponds to 200µm.

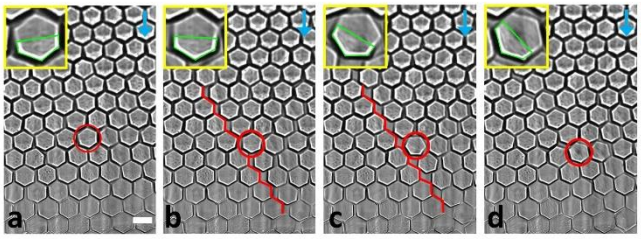

Fig. 7. Increasing mass of the depositing hexagons results in densification of already assembled structure which propagates along diagonal dislocations. The blue arrows indicate direction of sedimentation and the scale bar corresponds to 100µm.

of the well which leads to a non-uniform growth rate of the assembly. The areas of the fastest growth become unstable since they are not supported from the sides, which induces the redistribution of already assembled hexagons from the higher to the lower positions along the structure width (Fig. S4). The redistribution occurs through the dislocations of lines of hexagons along the diagonal boundaries. The Janus boundary of the individual hexagons typically remains oriented during this process; however, occasional rotation can be observed especially near defects already present in the structure (Fig. S5, video S5).

The third source of the misorientations in the structure is the relaxation of the translational disorders in the lower sections of the assembly. As more hexagons fall on the top of the assembly, the pressure applied on the hexagons at the lower section increases, which occasionally results in the rearrangement of local defects and the hexagon packing density locally increases. This initiates redistribution of all the hexagons above. The rearrangement occurs, as in the previous case, by dislocations of the lines of hexagons along the diagonal boundaries and, again, the orientation remained mostly preserved, however, a reorientation occasionally occurs (Fig. 7, video S6).

Self-assembly of other shapes

In the next section of our study, we tested whether similar densely packed crystalline assemblies can be obtained with other self-orienting building block shapes. SA of square-shaped Janus building blocks provided a densely packed square lattice with predominantly oriented Janus boundaries (Fig.8a). We observed long-range distortion in the structure – the boundaries between the individual squares are curved instead of straight, which is dictated by imperfect shapes of the building blocks – the PEGDA triangular part was somewhat larger than the PNIPAM one. The deformation originates from the deformation of the hydrogel squares – the PEGDA segment swells somewhat more than the PNIPAM one. Although the deformation is very small on a single particle level (~1 µm), it becomes substantial over longer distances in the densely packed assembly. The nonuniform swelling of the two respective halves is also present in the hexagons; however, it did not result in observable crystal structure distortion. However, the square block distortion may present an

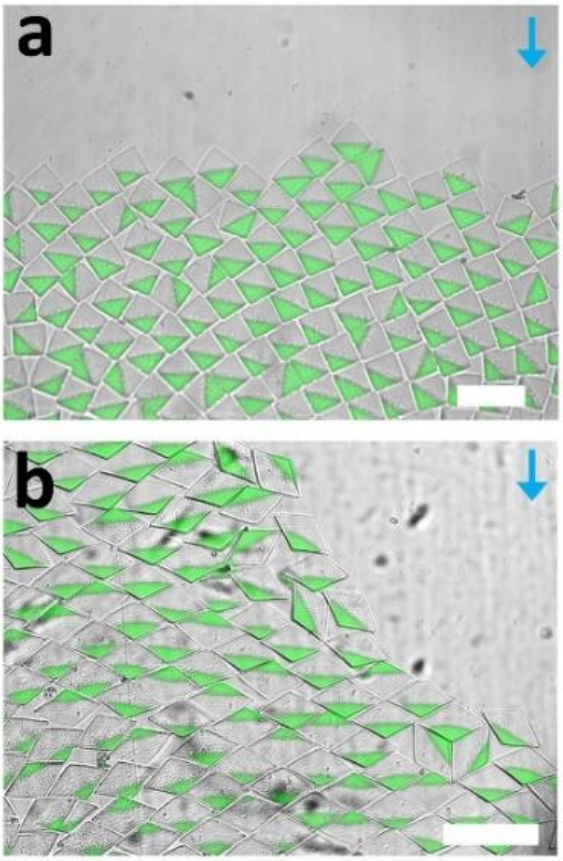

Fig. 8. Self-assembled (a) squares, (b) rhombuses. The PEGDA side is fluorescently labeled. The blue arrows indicate the sedimentation direction and the scale bar corresponds to 200μm.

opportunity to assemble dense packings on curved surfaces in the future.

Elongated hexagonal building blocks self-assembled into amorphous structures with only small domains with translational order. The reason lies in the low stability of the building block with respect to tipping - once the microgels reached the bottom, they tip over before other microgels could stabilize them from the sides (Fig. S6, video S7). Shortened – rhombic building blocks were stable with respect to tipping and, indeed, self-assembled into dense packing arrangements with translational order. However, their poor orientation during sliding (as described above) hindered their orientation order (Fig. 8b).

Furthermore, we studied the impact of a concave region on the self-assembly process by designing arrow-shaped microgels with a convex corner on the slippery side and a complementary concave region on the opposite side. The arrows formed interlocked chains during the sliding phase (Fig. S7, Supplementary text S3).

To indicate potential future applications of the presented self-assembled sheets, we bound the assembled hexagons covalently into a single sheet and, consequently, show its anisotropic shrinking/expansion in lateral dimension, when subjected to heating/cooling cycles. We were unable to prepare large scale sheets due to off-plane deformations of the sheet, occurring during the microgel binding, and hence, performed the experiment with only approximately twenty hexagons (Details can be found in ESI section SX).

In this work, we present a method for self-assembly of hydrogel tiles into void-less dense packings with translational and rotational order. The presented system does not possess the main feature of molecular/nanoscopic self-assembling systems - the ability of each building block to explore their phase space and repetitively switch between ordered-disordered positions to iteratively build the structure with locally minimized free energy. We show that even after complete removal of this self-corrective principle, ordered structures can be obtained. We demonstrated on examples of convex and concave polygons as building block shapes, which determinines whether the ordered structure is formed.

In the future experimentation, we plan to create more complex designs by multiplying the number of material segments in the microgels[41]. Additionally, we can locally tailor the crosslinking density within an individual microgel, by using a semitransparent mask during the SFL synthesis[43]. Such microgels would exhibit different swelling/shrinking behaviour and represent an opportunity for more complex programming of the anisotropic swelling response of the resulting structures (demonstrated e.g. in the ref. [48]) Furthermore, self-assembly on non-flat surfaces (e.g. bowl-shaped) may extent the variety of obtained microstructures. Moreover, microgels of multiple shapes can be assembled sequentially to obtain control over long-range changes in anisotropy

Conclusions

In summary, we present a simple method for the bottom-up formation of hydrogel sheets of structured two-material composition, through self-assembly of lithographic Janus building blocks. The polygon-shaped Janus microgel tiles are subjected to sliding on a tilted plane, self-orientate thanks to the nonuniform friction distribution and, subsequently they self-assemble into dense packings. As such, this strategy could be a robust method to create ordered materials and can be amenable to applications in microscale actuation or bottom-up tissue engineering. Furthermore, we recently demonstrated, that similar PNIPAM microgels, can be turned into actively crawling light-driven microrobots[44]. The combination of self-assembly with robotic micromanipulation can greatly increase the achievable complexity of fabricated structures.

Conflict of interest

There are no conflicts to declare.

Credit authorship contribution statement

Yadu Nath Vakkipurath Kodakkadan: Methodology, Data curation, Writing – original draft. **Charlie Maslen:** Writing – review & editing. **Petr Cigler:** Writing – review & editing, **Frantisek Stepanek:** Resources, Writing – review & editing. **Ivan Rehor:** Supervision, Conceptualization, Writing – review & editing.

Acknowledgments

The authors thank Dr. Pepijn Moerman for fruitful discussions over the manuscript. This project has received funding from the Junior GACR project No. 18-19170Y, and UCT Institutional Support of 'Marie Prochazkova' fund. I.R. acknowledges his J. E. Purkyne fellowship. The work of C.M. and Y.N.V.K. was supported by the grant of Specific University Research (Grant no. A1_FCHI_2020_005IG and A1_FCHI_2020_005). The work of P. C. was supported by the European Regional Development Fund; OP RDE; Project: "Chemical biology for drugging undruggable targets (Chem-BioDrug)" (no. CZ.02.1.01/0.0/0.0/16_019/0000729).

References

1 G. M. Whitesides and B. Grzybowski, *Science*, 2002, **295**, 2418–2421.
2 N. B. Crane, O. Onen, J. Carballo, Q. Ni and R. Guldiken, *Microfluid. Nanofluidics*, 2013, **14**, 383–419.
3 M. H. Lash, M. V. Fedorchak, S. R. Little and J. J. McCarthy, *Langmuir*, 2015, **31**, 898–905.
4 R. Gross and M. Dorigo, *Proc. IEEE*, 2008, **96**, 1490–1508.
5 K. Ariga, J. P. Hill, M. V. Lee, A. Vinu, R. Charvet and S. Acharya, *Sci. Technol. Adv. Mater.*, 2008, **9**, 014109.
6 S. Mann, *Nat. Mater.*, 2009, **8**, 781–792.
7 S. Biswas, M. Mozafari, T. Stauden and H. O. Jacobs, *Micromachines*, 2016, **7**, 54.
8 G. M. Whitesides and M. Boncheva, *Proc. Natl. Acad. Sci.*, 2002, **99**, 4769–4774.
9 M. Mastrangeli, G. Mermoud and A. Martinoli, *Micromachines*, 2011, **2**, 82–115.
10 B. Haghighat, M. Mastrangeli, G. Mermoud, F. Schill and A. Martinoli, *Micromachines*, 2016, **7**, 138.
11 T. G. Leong, A. M. Zarafshar and D. H. Gracias, *Small*, 2010, **6**, 792–806.
12 D. Karnaushenko, T. Kang and O. G. Schmidt, *Adv. Mater. Technol.*, 2019, **4**, 1800692.
13 L. Cademartiri, K. J. M. Bishop, P. W. Snyder and G. A. Ozin, *Philos. Trans. R. Soc. Lond. Math. Phys. Eng. Sci.*, 2012, **370**, 2824–2847.
14 A. B. Pawar and I. Kretzschmar, *Macromol. Rapid Commun.*, 2010, **31**, 150–168.
15 Q. Chen, S. C. Bae and S. Granick, *Nature*, 2011, **469**, 381–384.
16 M. Grzelczak, J. Vermant, E. M. Furst and L. M. Liz-Marzán, *ACS Nano*, 2010, **4**, 3591–3605.
17 M. Boncheva, D. A. Bruzewicz and G. M. Whitesides, *Pure Appl. Chem.*, 2003, **75**, 621–630.
18 M. Boncheva, S. A. Andreev, L. Mahadevan, A. Winkleman, D. R. Reichman, M. G. Prentiss, S. Whitesides and G. M. Whitesides, *Proc. Natl. Acad. Sci.*, 2005, **102**, 3924–3929.
19 Lash Melissa H., Jordan Jahnelle C., Blevins Laura C., Fedorchak Morgan V., Little Steven R., and McCarthy Joseph J., *Angew. Chem.*, 2015, **127**, 5952–5956.
20 M. Matsumoto and S. Hashimoto, *IEEE Trans. Autom. Sci. Eng.*, 2009, **6**, 385–391.
21 F. Ilievski, M. Mani, G. M. Whitesides and M. P. Brenner, *Phys. Rev. E*, , DOI:10.1103/PhysRevE.83.017301.
22 U. Okabe, T. Okano and H. Suzuki, *Sens. Actuators Phys.*, 2017, **254**, 43–53.
23 H. Wu, V. R. Thalladi, S. Whitesides and G. M. Whitesides, *J. Am. Chem. Soc.*, 2002, **124**, 14495–14502.
24 J. Deseigne, O. Dauchot and H. Chaté, *Phys. Rev. Lett.*, 2010, **105**, 098001.
25 C. A. Weber, T. Hanke, J. Deseigne, S. Léonard, O. Dauchot, E. Frey and H. Chaté, *Phys. Rev. Lett.*, 2013, **110**, 208001.
26 Fernandez Javier G. and Khademhosseini Ali, *Adv. Mater.*, 2010, **22**, 2538–2541.
27 D. J. Kraft, R. Ni, F. Smallenburg, M. Hermes, K. Yoon, D. A. Weitz, A. van Blaaderen, J. Groenewold, M. Dijkstra and W. K. Kegel, *Proc. Natl. Acad. Sci.*, 2012, **109**, 10787–10792.
28 M. Mastrangeli, Q. Zhou, V. Sariola and P. Lambert, *Soft Matter*, 2017, **13**, 304–327.
29 S. Yoshida, M. Takinoue, E. Iwase and H. Onoe, *J. Appl. Phys.*, 2016, **120**, 084905.
30 J. J. Crassous, A. M. Mihut, E. Wernersson, P. Pfleiderer, J. Vermant, P. Linse and P. Schurtenberger, *Nat. Commun.*, 2014, **5**, 5516.
31 Z. Ma, A. W. Holle, K. Melde, T. Qiu, K. Poeppel, V. M. Kadiri and P. Fischer, *Adv. Mater.*, **n/a**, 1904181.
32 S. E. Chung, W. Park, S. Shin, S. A. Lee and S. Kwon, *Nat. Mater.*, 2008, **7**, 581–587.
33 Kraus T., Malaquin L., Delamarche E., Schmid H., Spencer N. D., and Wolf H., *Adv. Mater.*, 2005, **17**, 2438–2442.
34 P.-Y. Wang and T. G. Mason, *Nature*, 2018, **561**, 94–99.
35 T. M. Schneider, S. Mandre and M. P. Brenner, *Phys. Rev. Lett.*, , DOI:10.1103/PhysRevLett.106.094503.
36 M. Krishnan, M. T. Tolley, H. Lipson and D. Erickson, *Phys. Fluids*, 2008, **20**, 073304.
37 J. Zemánek, T. Michálek and Z. Hurák, *Lab. Chip*, 2018, **18**, 1793–1801.
38 W. Yang, H. Yu, G. Li, Y. Wang and L. Liu, *Small*, 2016, n/a-n/a.
39 B. D. Fairbanks, M. P. Schwartz, C. N. Bowman and K. S. Anseth, *Biomaterials*, 2009, **30**, 6702–6707.
40 D. C. Pregibon, M. Toner and P. S. Doyle, *Science*, 2007, **315**, 1393–1396.
41 J. Lee, P. W. Bisso, R. L. Srinivas, J. J. Kim, A. J. Swiston and P. S. Doyle, *Nat. Mater.*, 2014, **13**, 524–529.

42 D. Dendukuri, S. S. Gu, D. C. Pregibon, T. A. Hatton and P. S. Doyle, *Lab. Chip*, 2007, **7**, 818–828.
43 Y. N. V. Kodakkadan, K. Idzakovicova, J. Sepitka, D. ten Napel, E. Safai, P. Cigler, F. Štěpánek and I. Rehor, *Biomater. Sci.*, , DOI:10.1039/C9BM02056J.
44 I. Rehor, C. Maslen, P. G. Moerman, B. G. P. van Ravensteijn, R. van Alst, J. Groenewold, H. B. Eral and W. K. Kegel, *Soft Robot.*, 2020, soro.2019.0169.
45 P. C. Nalam, S. N. Ramakrishna, R. M. Espinosa-Marzal and N. D. Spencer, *Langmuir*, 2013, **29**, 10149–10158.
46 T. Kreer, *Soft Matter*, 2016, **12**, 3479–3501.
47 A. A. Pitenis, J. M. Urueña, K. D. Schulze, R. M. Nixon, A. C. Dunn, B. A. Krick, W. G. Sawyer and T. E. Angelini, *Soft Matter*, 2014, **10**, 8955–8962.
48 J. Kim, J. A. Hanna, M. Byun, C. D. Santangelo and R. C. Hayward, *Science*, 2012, **335**, 1201–1205.
49 D. Dendukuri, P. Panda, R. Haghgooie, J. M. Kim, T. A. Hatton and P. S. Doyle, *Macromolecules*, 2008, **41**, 8547–8556.
50 I. Hutchings and P. Shipway, *Tribology: Friction and Wear of Engineering Materials*, Butterworth-Heinemann, 2017.
51 Y. Du, E. Lo, S. Ali and A. Khademhosseini, *Proc. Natl. Acad. Sci.*, 2008, **105**, 9522–9527.
52 T. Canal and N. A. Peppas, *J. Biomed. Mater. Res.*, 1989, **23**, 1183–1193.

Notes and references

‡ Footnotes relating to the main text should appear here. These might include comments relevant not central to the matter under discussion, limited experimental and spectral data, and crystallographic data.
§
§§
etc.

Supplementary information

Friction-Directed Self-Assembly of Janus Lithographic Microgels into Anisotropic 2D Structures

Yadu Nath Vakkipurath Kodakkadan, [a] Charlie Maslen, [a] Petr Cigler, [b] Frantisek Stepanek, [a] Ivan Rehor[*,a,b]

[a] University of Chemistry and Technology Prague, Faculty of Chemical Engineering,Technicka 5, 166 28 Prague 6, Czech Republic

[b] Institute of Organic Chemistry and Biochemistry of the Czech Academy of Sciences, Flemingovo nam. 2, 160 00, Prague, Czech Republic

[*] e-mail: ivan.rehor@vscht.cz

Supplementary text S1:

Sliding at various angles:

At the tilt angles 3°, 6°, and 9°, the reorientation occurred over a traveled distance corresponding to several microgel diameters, while at 12° the reorientation took more distance and time. Furthermore, we observed different equilibrium angle of sliding hexagonal microgels at 12° – instead of sliding the PEGDA side first, they slide tilted by 60° with respect to this position (Fig. S3). Apparently, new phenomena are participating under the high tilt angle. We hypothesize these may originate from non-perfectly flat microgels (The PEGDA side is somewhat thicker ~1-2 µm due to somewhat higher photo-reactivity of the PEGDA pregel compared to the PNIPAM pregel[49]) which causes mild tilt of the hydrogel and so can generate lift force[50]. However, for the angles 10° and below, the microgels self-orientate the PEGDA side down-the slope.

Supplementary text S2:

Self-orientation rates of Janus hydrogels of different shapes

The rate of self-orientation of a microgel depends on the torque, given by the separation between the center of mass and the center of friction. Both microgels are of very similar density and, thus we assume the center of mass to be at the geometrical center of the polygon. The center of friction for a sheared plane, composed from a single material will be identical to the center of mass, as we state in the main text. Hence, to find the center of friction of the whole polygon, we first calculate the distance (d) between the center of friction/mass of the half of the polygon of uniform composition and the geometrical center/center of mass of the whole polygon. The distance between the center of friction of the whole Janus microgel and its center of mass (δ) can be calculated from these two uniform-composition centers in an analogy to the center of mass.

$$\delta = d \cdot (f_1 + \frac{f_2}{f_1}) + f_2 \qquad \text{(S1)}$$

Where f_1 and f_2 are friction forces of the respective halves of the microgel. Since the material compositions are constant (PEGDA and PNIPAM, respectively) and the polygons and the sheared areas are identical, the f_1 and f_2 are constant and the only variable in the equation is d. The larger is the d, i.e. the longer the particle in the direction perpendicular to the interphase boundary, the greater is the difference between the center of mass and the center of friction, which ultimately results in greater torque.

All values below are derived using simple geometrical principles and thus the derivations are not shown in detail. For a regular hexagon of an edge length a, the distance d is $\frac{7}{18}a$ ($0.389a$). An isoareal square to the hexagon of an edge a has edge length b equal to $\sqrt{3 \cdot \left(\frac{\sqrt{3}}{2}\right)} \cdot a$. The

distance between the center of mass and the center of mass of half of such square, divided along its diagonal is equal to $\frac{1}{3\cdot\sqrt{2}}\cdot b$ which corresponds to approximately $0.379a$. Since the lower d results in the lower mass δ and, ultimately, in lower torque, the square is expected to rotate slower, than the hexagon. For isoareal rhombus, the d is equal to $0.289a$, which, as showed in the sliding experiments, is not sufficient separation to achieve a self-orientation. On the other hand, for the elongated hexagon (two parallel edges have double-length; all angles are equal to 120°) the d is $0.838a$ and these hexagons rapidly self-oriented in conducted experiments.

Supplementary text S3:

We studied the impact of a concave region on the self-assembly process by designing arrow-shaped microgels with a convex corner on the slippery side and a complementary concave region on the opposite side. The arrows formed interlocked chains during the sliding phase (Fig. S7a, video S8). This phenomenon originates from non-uniform sliding velocities of the individual microgels – when the faster microgel reaches the slower one, they interlock and continue as a chain. The variation in microgels' sliding speeds originates from their synthesis. The position of the PEGDA-PNIPAM pregel boundary would oscillate somewhat during the microfluidic fabrication, which resulted in variable PEGDA-PNIPAM gel ratio in each microgel particle and ultimately in variation in their sliding speeds. Naturally, the microgel chains collapsed at the bottom of the well forming a random assembly (Fig. S7b).

In the next section of this work, we show a potential way to use the demonstrated assembling system for the fabrication of 2D micropatterned soft materials. The microgels in selected areas of the self-assembly can be bound covalently together into a single sheet using remnant acrylate moieties present in the hydrogel. A similar methodology has been previously used for covalent binding of acrylate microgels[26,51]. The microgels are composed of PNIPAM, crosslinked with PEGDA and pure PEGDA respectively. Some of the PEGDA molecules are incorporated into only a single polymeric chain during the microgel synthesis and, thus, contain one unreacted acrylate moiety which can be used for the covalent binding. To perform the reaction, LAP photoinitiator was added to the well and the assembly was irradiated with UV light to initiate radical polymerization of the remnant acrylates. These remnant acrylates come from either two adjacent microgels, which results in the discs binding or, alternatively, they are present within a single microgel and the newly formed, internal, crosslinks densify the hydrogel network, which results in isotropic shrinkage of the microgel[52]. Both these processes occur simultaneously, so the microgels bind into a single sheet while their linear dimensions reduce by ~20 %.
The resulting sheet is composed of spatially organized segments of PEGDA and PNIPAM respectively. Since the PNIPAM is thermoresponsive, these segments will undergo isotropic shrinkage upon heating while the PEGDA ones will keep constant volume. As a result, the entire sheet will shrink anisotropically, given by the spatial arrangement of the respective segments. The non-responsive PEGDA sections are connected into stripes, which are responsible for lower shrinkage in the direction parallel to these ribbons, than the perpendicular one. Indeed, we observed anisotropic shrinkage rates in the perpendicular directions of the sheet, subjected to heating-cooling (Fig. S8). This experiment indicates the potential future application of micropatterned sheets in microscale actuation, however, it will require a theoretical understanding of the mechanics of the process to gain predictive power over the programming of the anisotropic response through designing of the building block shapes

Supplementary figures:

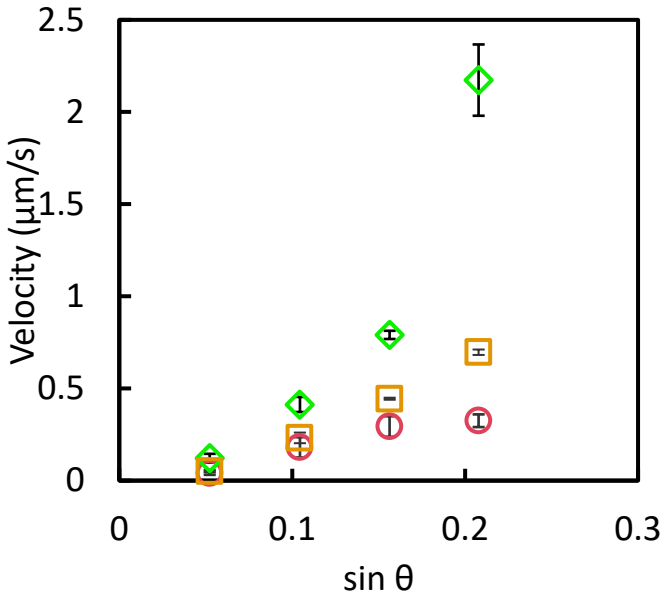

Fig. S1. Sliding velocities of microgels, composed from single-phase PNIPAM (circles) and PEGDA (diamonds) hydrogel, and Janus PNIPAM-PEGDA microgels (squares) at angles 3°, 6°, 9°, and 12° respectively. We ascribe the intercept present at the x axis (the zero velocity would correspond to the tilt angle around 2°) to a static friction contribution. The error bars represent standard deviation from 10 experiments.

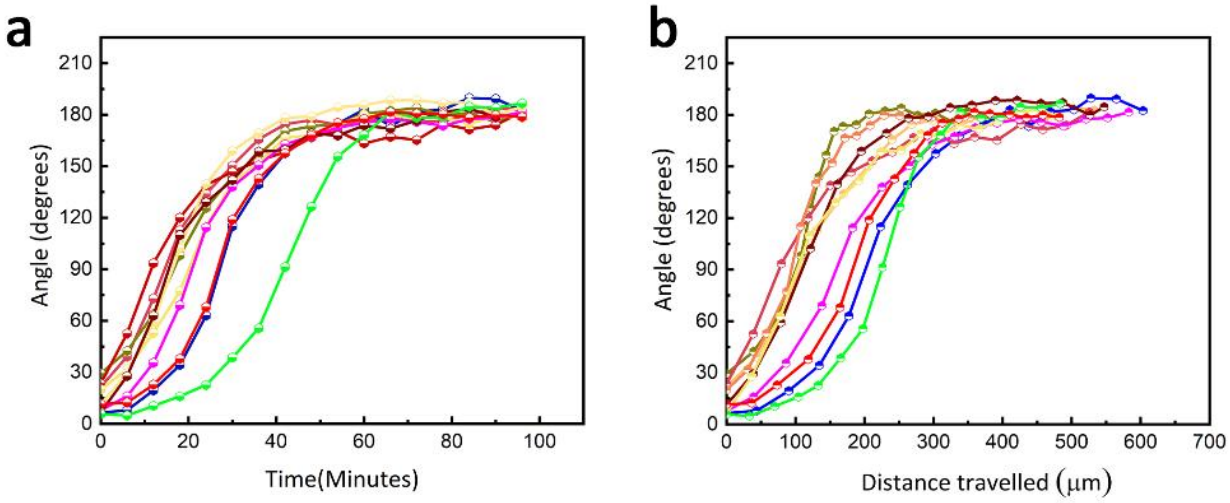

Fig. S2. Reorientation of Janus hexagons at 6° tilt as a function of a. Time, b. Traveled distance, respectively. To observe the orientation change in the entire 180° range, the hexagons were preoriented by tilting the well in the opposite direction.

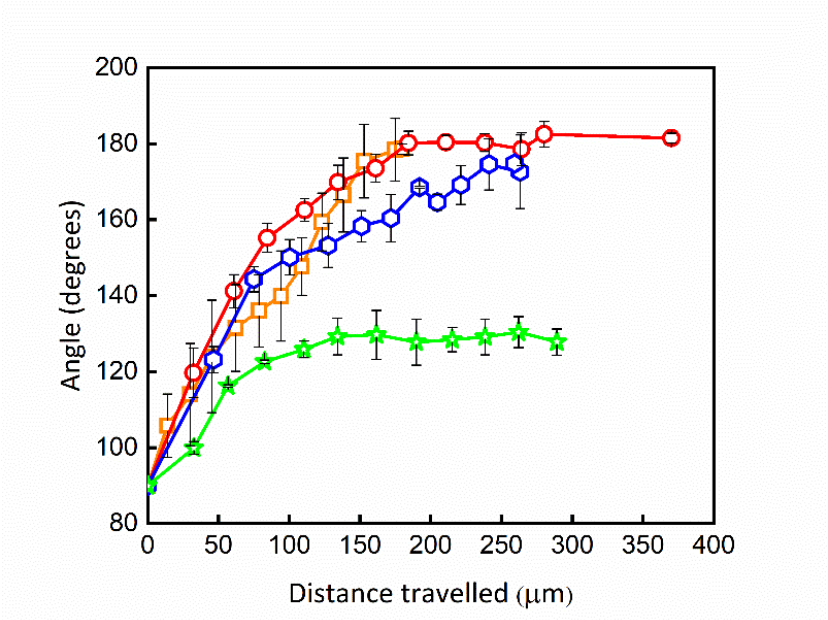

Fig. S3. Sliding hexagons – images show gradual alignment of the Janus hexagons on a 3° (orange rectangle), 6° (red circle), 9° (blue hexagon), 12° (green star) slopes. Only the second half of the reorientation is plotted, i.e. the initial orientation the Janus boundary is parallel to the sliding direction.

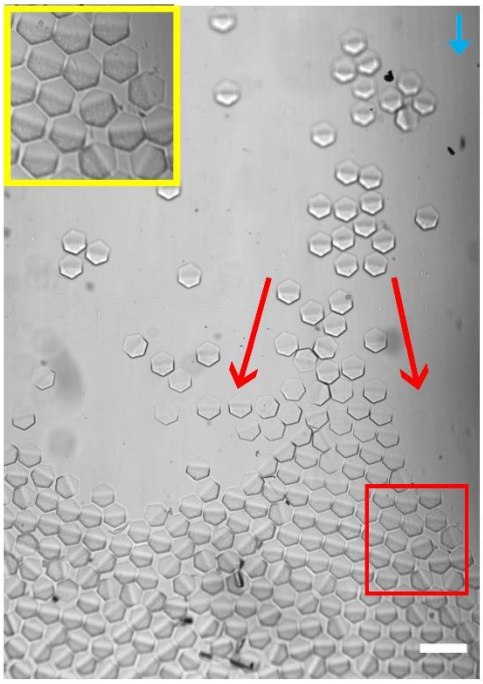

Fig. S4. The irregular distribution of the sliding hexagons along the sedimentation well width results in their redistribution after reaching the structure (indicated by the red arrows, the blue arrow indicates the sedimentation direction, red rectangle indicates the area depicted in Figure S5, the scale bar corresponds to 200 μm).

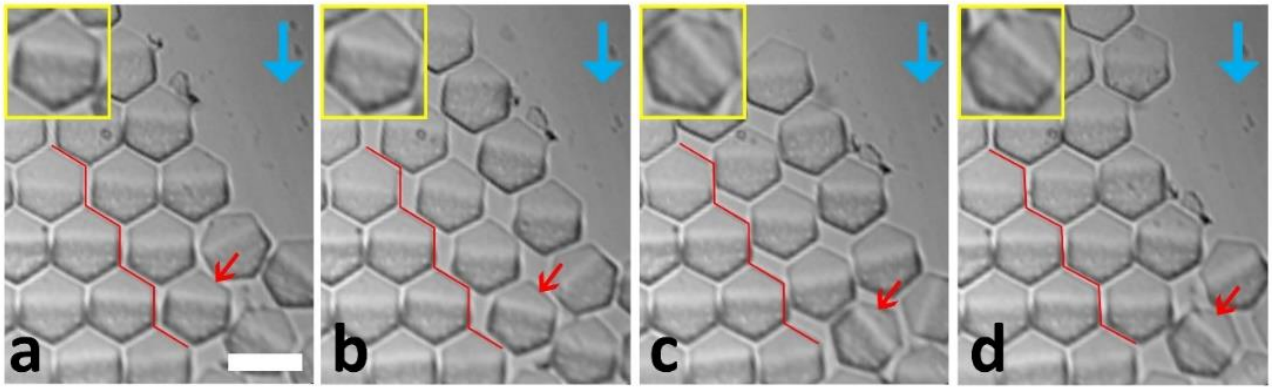

Fig. S5. Orientation loss during building block redistribution near a defect. The red zigzag line indicates the dislocation line; red arrow highlights the hexagon with the lost orientation. The blue arrow indicates sedimentation direction. The scale bar corresponds to 100 µm.

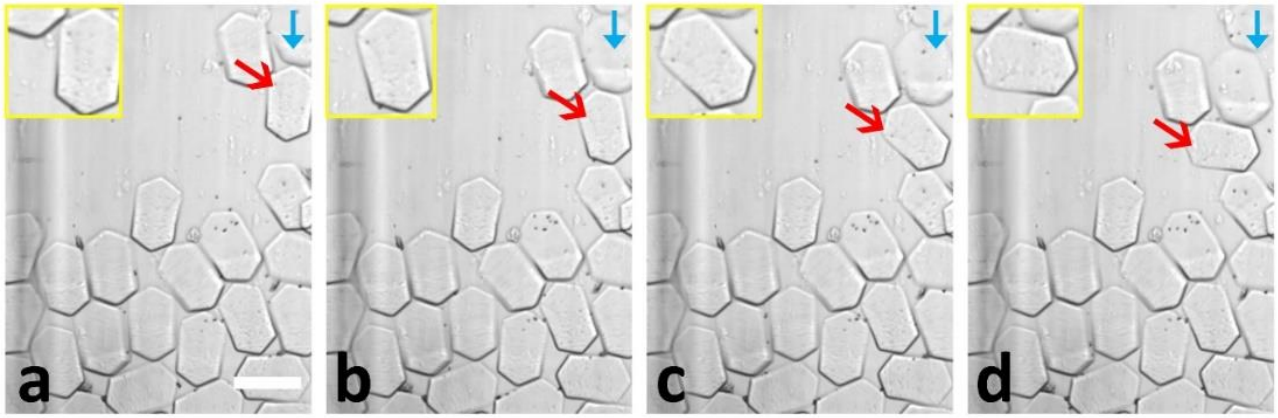

Fig. S6. Error on incorporation due to tipping over of elongated hexagon microgels. The blue arrow indicates sedimentation direction; the scale bar corresponds to 200 µm.

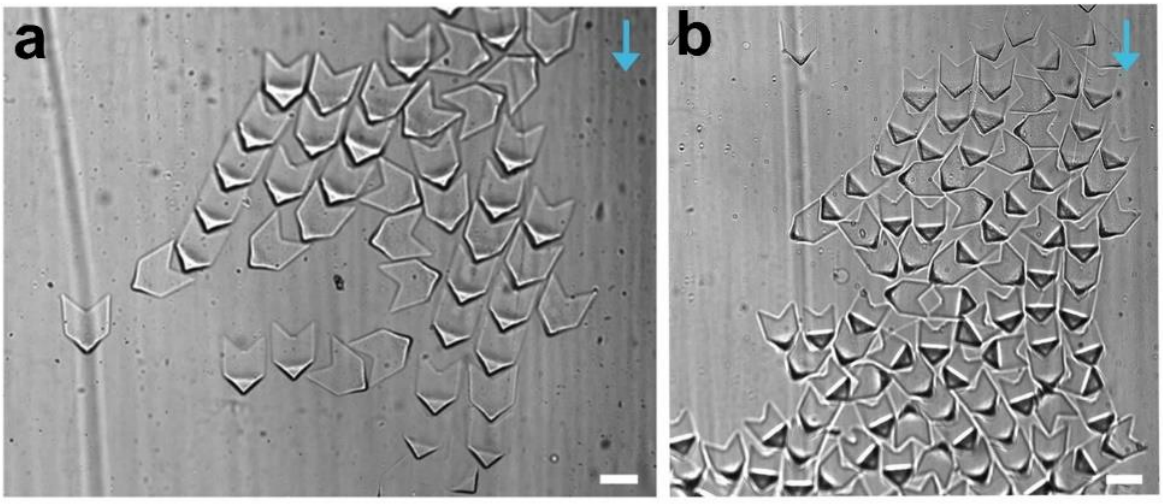

Fig. S7. (a) Interlocked chains of arrow-shaped microgels (b) The V-shaped particle assembly. The blue arrow indicates the sedimentation direction; the scale bar corresponds to 100 µm.

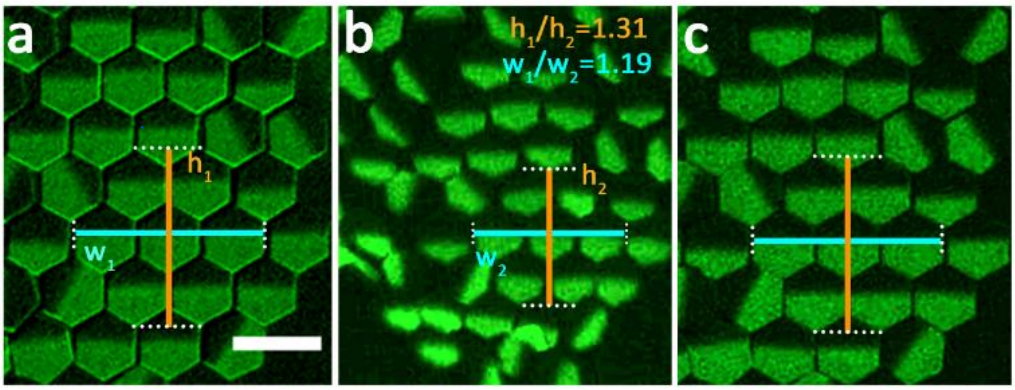

Fig. 9. Anisotropic deformation of microgel sheet, subjected to heating and cooling. (a) 25, (b) 60, (c). 25 °C. Scale bar corresponds to 100 μm.